
Enhancing Interaction Modeling with Agent Selection and Physical Methods for Trajectory Prediction

Shiji Huang, Lei Ye*, Min Chen, Wenhai Luo,
Chenqi Xu, Deyuan Liang, Dihong Wang
Zhejiang University of Technology
{201806150307, yelei}@zjut.edu.cn

Abstract

In this study, we address the limitations inherent in most existing vehicle trajectory prediction methodologies that indiscriminately incorporate all agents—exclusively at present—within a predetermined proximity when accounting for inter-agent interactions. These approaches commonly employ attention-based architecture or graph neural networks for encoding interactions, which introduces three challenges: (i) The indiscriminate selection of all nearby agents substantially escalates the computational demands of the model, particularly in those interaction-rich scenarios. (ii) Moreover, the simplistic feature extraction of current time agents falls short of adequately capturing the nuanced dynamics of interactions. (iii) Compounded by the inherently low interpretability of attention mechanism and graph neural networks, there is a propensity for the model to allocate unreliable correlation coefficients to certain agents, adversely impacting the accuracy of trajectory predictions. To mitigate these issues, we introduce ASPILin, a novel approach that enhances the selection of interacting agents by considering their current and future lanes, extending this consideration across all historical frames. Utilizing the states of the agents, we estimate the nearest future distance between agents and the time needed to reach this distance. Then, combine these with their current distances to derive a physical correlation coefficient to encode interactions. Experiments conducted on popular trajectory prediction datasets demonstrate that our method is efficient and straightforward, outperforming other state-of-the-art methods. Code is available at <https://github.com/kkk00714/ASPILin>.

1 Introduction

Accurately forecasting the trajectories of human-driven vehicles and pedestrians sharing the environment with autonomous vehicles is paramount within autonomous driving[16]. Such precise trajectory predictions are indispensable for downstream intelligent planning systems to make informed decisions, thereby significantly improving autonomous driving operations' safety, comfort, and efficiency. However, due to the inherent uncertainty and the multi-modal nature of driving behaviors, vehicle trajectory prediction against an urban setting presents significant challenges that include, but are not limited to, spatiotemporal modeling of historical trajectories[64], inter-agent interaction modeling[39, 64, 50, 24], environmental description[9], kinematic constraints[50, 19], and real-time inference[60].

Many trajectory prediction methods based on deep learning have emerged in recent years, supplanting the early purely physics- and maneuver-based methods[62, 49]. This shift is attributable to physics- and maneuver-based methods being only suitable for simple prediction scenarios and short-term

*Corresponding author

forecasts (not exceeding 1 second). In contrast, deep learning-based methods can consider physics-related, road-related, and interaction-related factors and adapt to more complex scenes[17]. The highly interactive nature of vehicles makes modeling interactions a critical component in vehicle trajectory prediction. Although there has been considerable research (see more details in App. A) dedicated to modeling vehicle-agent interactions, there are still three significant shortcomings:

(i) *Overly simplistic agent selection.*

As shown in Fig. 1, nearly all previous methods indiscriminately select agents surrounding the target vehicle (or even all agents from the scene) into the interaction model. This is reasonable for pedestrian trajectory prediction[46, 12], given the more random nature of pedestrian movements. Vehicle movements, however, are governed by more stringent regulatory constraints, such as traffic signals and designated lanes, enabling a more refined selection of interacting agents.

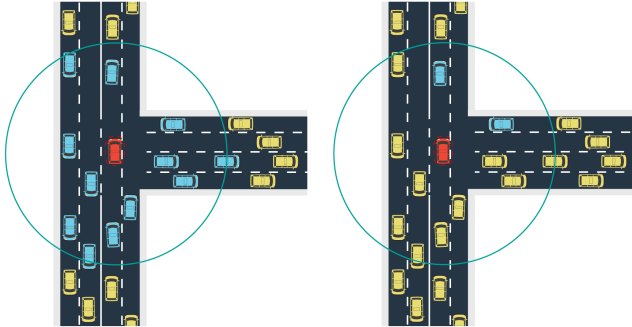


Figure 1: **Left:** due to the simplistic selection of interacting agents (blue), the model is forced to process some spurious interactions, such as vehicles moving in the opposite direction on the road to the left of the target vehicle (red). **Right:** further selection allows the model to concentrate exclusively on meaningful interactions, depicted in the figure as the vehicle positioned ahead within the same lane and those poised to merge with the target vehicle (assuming the target vehicle is not preparing to change lanes).

(ii) *Ignoring dynamic interactions.*

On the temporal scale, many approaches focus their attention solely on agents at the current timestep[64, 60, 11, 39, 24]. Indeed, the interaction events at the current time step are most likely to affect the future trajectory of the target vehicle. However, this also means that the model might fail to capture the complexity of dynamic interactions fully. If an agent significantly influences the behavior of the target vehicle early in the observation sequence, focusing solely on the current timestep could miss such an impact. This hinders the model from learning the full interaction causality, particularly for prediction tasks with longer observation sequences.

(iii) *Interaction modeling with low interpretability.*

Attention mechanism[20, 60, 38] and Graph Neural Network (GNN)[25, 63] are popular in numerous interaction-aware methods. Although they aid in improving model performance, fundamentally, these methods do not elucidate the underlying decision logic or cognitive processes. Theoretically, the extent of interaction among agents is highly correlated with their intentions and physical representations and should depend on both aspects simultaneously. For instance, compared to agents that are closer but have mismatched intentions, agents further away but on a merging path with the target vehicle may exhibit greater interaction. Relying on existing methods to fully deduce such complex causal relationships is extremely difficult, as they must consider concurrently agents’ intentions and physical representations.

Considering the connections among the three: For (i) and (ii), using a more extensive selection range for agents[64, 60, 11] could reduce the likelihood of overlooking dynamic interactions, but it also increases the complexity of modeling. Conversely, methods that utilize a smaller selection range[39, 24] struggle to capture dynamic interactions fully. For (i) and (iii), simultaneously leveraging the intentions of agents and their physical representations is unrealistic, as the intentions of agents are not known beforehand. However, if agents with matching intentions could be identified in advance, then it would only be necessary to consider their physical representations when modeling interactions. To this end, we propose a more refined scheme for agent selection. It uses the intended future lanes of each agent as a proxy for their intentions and combines this with their current lane to select up to four interacting agents. Then, by estimating the time required for agents to reach their nearest positions through their states and combining this with their mutual distances, we derive a novel correlation coefficient, which replaces the attention score and is integrated into the Transformer architecture. To fully capture the dynamic interactions, we apply the agent selection process to every timestep of the historical sequence. This involves extracting the features of agents in each frame and concatenating them to serve as the input to the model. Specifically, the input comprises the continuous trajectory of the target vehicle and the trajectory segments of four different types of agents. These trajectory segments of each type may be discontinuous since they could originate from different agents. Finally,

we utilized reparameterization to construct a simple Conditional Variational Autoencoder (CVAE) framework for predicting the future trajectories of vehicles.

The contributions of our work are the following:

- To our knowledge, our work is the pioneering effort to refine the interacting agent selection, and it is based on a lane predictor and four mutually exclusive rules.
- An interaction representation paradigm, where the input includes the states of the target vehicle and the states of its interacting agents at each observation timestep but not only the current timestep.
- A novel physics-based method for calculating correlation coefficient, replacing the attention score and integrated into the Transformer architecture.

2 Method

In this section, we initially discuss the single-agent trajectory prediction problem, followed by a specific introduction to the interaction module of the model proposed. Details on other crucial modules and the training procedure can be found in App. B. An overview of our proposed framework is illustrated in Fig. 2. We named it ASPILin, emphasizing agent selection, physical interaction, and linear temporal weights.

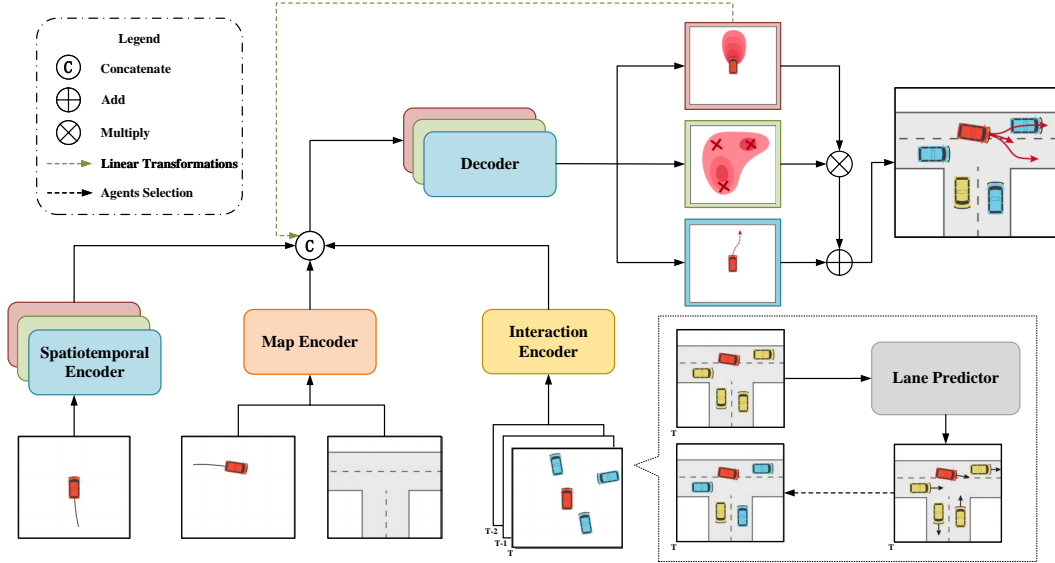


Figure 2: ASPILin starts by predicting the future lanes for all agents in the scene for each timestep via a lane predictor, then selects up to four different types of interacting agents based on their current and future lanes. The states of the target vehicle and interacting agents across all timesteps are extracted and concatenated to serve as input for the interaction encoder. Meanwhile, the historical states of the target vehicle in the relative and absolute coordinate systems, along with the rasterized scene map, serve as inputs for the spatiotemporal encoder and the map encoder, respectively. The decoder first outputs the mean and variance of the future trajectory of the target vehicle, followed by using the variance for sample forecasting. Reparameterization is ultimately employed to generate multi-modal future trajectories of the target vehicle.

2.1 Problem Formulation

Single-agent trajectory prediction is designed to forecast the future trajectory of a target vehicle conditioned on agents' historical states X and the map of scene \mathcal{M} . To be more specific, we assume that at time t , there are N agents (vehicles, pedestrians, cyclists) in the scene, so their historical

states can be represented as $X_t = [x_t^1, x_t^2, \dots, x_t^N] \in \mathbb{R}^{N \times 7}$, where x_t^n is the state of agent n at time t , including xy coordinates ($p_t^n \in \mathbb{R}^2$), heading angle ($h_t^n \in \mathbb{R}$), speed ($v_t^n \in \mathbb{R}^2$), and acceleration ($a_t^n \in \mathbb{R}^2$). Specifically, x_t^1 represents the state of the target vehicle at time t . Taking into account T_h historical observation timesteps, the overall historical state of the agents is denoted as $X = [X_{-T_h+1}, X_{-T_h+2}, \dots, X_0] \in \mathbb{R}^{N \times T_h \times 7}$. Similarly, the future ground-truth trajectory of the target vehicle is defined as $Y = [y_1, y_2, \dots, y_{T_f}] \in \mathbb{R}^{T_f \times 2}$ over T_f timesteps, where y_t is the xy coordinates at time t . To forecast multi-modal future trajectories, the predicted trajectory of K modes is denoted as $\hat{Y} = [\hat{Y}^1, \hat{Y}^2, \dots, \hat{Y}^K] \in \mathbb{R}^{K \times T_f \times 2}$. Our goal is to learn a generative model to parameterize the distribution $\mathcal{P}(Y|X, \mathcal{M})$.

2.2 Interaction Module

Our research primarily concentrates on the interaction module. Since trajectory prediction is fundamentally a form of time series forecasting, it is crucial to account for the spatiotemporal connectivity of inter-agent interactions. Therefore, we further divide the interaction module into interacting agent selection (spatial), interaction representation (temporal), and interaction modeling (both).

Interacting Agent Selection We define the Euclidean distance between agent i ($i > 1$) and the target vehicle at time t as d_t^i . If d_t^i falls below a manually defined range threshold \mathcal{D} (typically, the setting of \mathcal{D} should be positively correlated with T_f), it is considered that there is a potential for interaction between agent n and the target vehicle. This is just a preliminary filtering, but previous works stopped here. We now proceed to a further selection.

In urban areas, vehicles operate within lanes while driving, which allows us to convert the problem of interaction between agents into a correlation problem between lanes. At time t , the lane to which agent i belongs is defined as l_t^i . As time passes, the agent will move to another lane, which we refer to as future lane l_{t+}^i ($t+ \leq T_f$). Because the size of each scene is finite, if l_t^i represents the last lane traversed by agent n in the scene, then it is stipulated that $l_{t+}^i = l_t^i$. The future lane l_{t+}^i can be easily captured for training data. However, a lane predictor must be built at the inference stage to predict l_{t+}^i . Intuitively, since each scene has a finite number of lanes, predicting the future lane can easily be converted into a classification problem, represented as $l_{t+}^i = f_{\text{clf}}([x_t^i, l_t^i])$. Nevertheless, this method is unsuitable for real-world applications as it only accommodates predictions in scenarios with training. For this purpose, we propose using an ultra-lightweight model to forecast unimodal medium-to-high-precision all types of agents' trajectories for future moments, subsequently mapping each timestep's trajectory onto the respective lane. The entire process can be expressed as $\{l_k^i\}_{k=-T_h+1}^0 = g(f_{\text{reg}}(\{x_k^i\}_{k=-T_h+1}^0, \mathcal{M}))$, where g is the mapping from trajectory to lane. One

challenge of using this regression method is that agents in a real-world scenario sometimes have different observation steps. Yet, the model must predict the trajectories of all agents to ensure the accuracy of the interacting agent selection. Therefore, during inference, we use a Constant Acceleration

Algorithm 1 Interacting agent selection algorithm

Input: Agents' state at time t $X_t \in \mathbb{R}^{N \times 7}$, Agents' current and future lanes at time t $L_t \in \mathbb{R}^{N \times 2}$, Range threshold \mathcal{D}

Output: Index list \mathcal{N}

- 1: Extract position P_t and velocity V_t from X_t ;
 - 2: Initialize min-distance $d_{\text{SL}}, d_{\text{FL}}, d_{\text{FF}}, d_{\text{ML}} \leftarrow \mathcal{D}$;
 - 3: Initialize neighbor index list $\mathcal{N} \leftarrow [0, 0, 0, 0]$;
 - 4: **for** each agent $i \leftarrow 2$ **to** N **do**
 - 5: Distance $d_t^i \leftarrow \|p_t^i - p_t^1\|_2$;
 - 6: Orientation $o_t^i \leftarrow (p_t^i - p_t^1) \cdot v_t^1$;
 - 7: **if** $d_t^i < d_{\text{SL}}$ and $l_t^i = l_t^1$ and $o_t^i \geq 0$ **then**
 - 8: $d_{\text{SL}} \leftarrow d_t^i$;
 - 9: $\mathcal{N}[0] \leftarrow i$;
 - 10: **else if** $d_t^i < d_{\text{FL}}$ and $l_t^i = l_{t+}^1$ and $o_t^i \geq 0$ and $l_{t+}^1 \neq l_t^1$ **then**
 - 11: $d_{\text{FL}} \leftarrow d_t^i$;
 - 12: $\mathcal{N}[1] \leftarrow i$;
 - 13: **else if** $d_t^i < d_{\text{FF}}$ and $l_t^i = l_{t+}^1$ and $o_t^i < 0$ and $l_{t+}^1 \neq l_t^1$ **then**
 - 14: $d_{\text{FF}} \leftarrow d_t^i$;
 - 15: $\mathcal{N}[2] \leftarrow i$;
 - 16: **else if** $d_t^i < d_{\text{ML}}$ and $l_t^i = l_{t+}^1$ and $o_t^i \geq 0$ and $l_{t+}^1 \neq l_t^1$ **then**
 - 17: $d_{\text{ML}} \leftarrow d_t^i$;
 - 18: $\mathcal{N}[3] \leftarrow i$;
 - 19: **end if**
 - 20: **end for**
 - 21: **return** $\mathcal{N}, d_{\text{SL}}, d_{\text{FL}}, d_{\text{FF}}, d_{\text{ML}}$;
-

(CA) model $\text{CA}(\cdot)$ to pad the missing observation steps for agents:

$$\text{CA}(t; p_t^i, v_t^i, a_t^i) = p_t^i + v_t^i t + \frac{a_t^i}{2} t^2. \quad (1)$$

For an agent i whose states $\{x_k^i\}_{k=t_1}^{t_2}$ ($-T_h + 1 < t_1 \leq t_2 < 0$) are missing observation steps, the most recent state is used as the input for $\text{CA}(\cdot)$:

$$\{x_k^i\}_{k=-T_h+1}^{t_1-1} = \text{CA}(t; x_{t_1}^i), t \in \{-T_h + 1 - t_1, \dots, -1\}. \quad (2)$$

Similarly, we can derive:

$$\{x_k^i\}_{k=t_2+1}^0 = \text{CA}(t; x_{t_2}^i), t \in \{1, \dots, -t_2\}. \quad (3)$$

The model $f_{\text{reg}}(\cdot)$ is implemented as a simplified version of ASPILin, excluding the interaction module, and we named it Lin. Only data containing all historical and future timesteps is used to train Lin to guarantee the model’s performance.

If the distance between two agents is less than \mathcal{D} and their current and future lanes intersect, they are highly likely to interact. As described in Alg. 1, we further select four different types of interacting agents: *Same lane and Leading* (SL), *Future lane and Leading* (FL), *Future lane and Following* (FF), and *Merging and Leading* (ML). Suppose the angle between the agent’s position relative to the target vehicle and the target vehicle’s heading does not exceed 90° . In that case, the agent is considered leading the target vehicle. Additionally, to determine FL and FF, it must be ensured that the target vehicle is not traveling in the last lane; otherwise, its future lane is meaningless, which could lead to FL intersecting with SL. Similarly, this reasoning holds for ML. Finally, the agent closest to the target vehicle in each category is selected as its interacting agent.

Interaction Representation Once the method for interacting agent selection is established, the next step is to create an interaction representation to serve as the input for the interaction encoder. A common practice is to select four types (SL, FL, FF, and ML) interacting agents i_1 to i_4 for the target vehicle at $t = 0$ and then their historical states, denoted as $I = [\{x_k^1\}_{k=-T_h+1}^0, \{\{x_k^{i_n}\}_{k=-T_h+1}^0\}_{n=1}^4] \in \mathbb{R}^{5 \times T_h \times 7}$. However, this method encounters a predicament similar to the Lin model, which involves padding for agents with missing observation steps. Whether zero values are used or the state values from the nearest timestep[39] are employed for padding, the model inevitably processes distorted data during training. Although some approaches[60] employ a mask during encoding to disregard missing timesteps, the interaction representation of the target vehicle throughout the observation steps remains incomplete. Additionally, the interacting agents at $t = 0$ may not have interacted with the target vehicle in the early stages of observation.

An ideal interaction representation should be able to show the interactions of the target vehicle at each historical timestep, which facilitates the model’s learning of the causal relationship between interactions and future trajectories. Thus, we introduce a novel paradigm for interaction representation, defined as $I = [I^1, (I^s)_{s \in \mathcal{S}}] \in \mathbb{R}^{5 \times T_h \times 7}$, where $I^n = [x_{-T_h+1}^n, x_{-T_h+2}^n, \dots, x_0^n] \in \mathbb{R}^{5 \times 7}$ represents the states of type n agents in all observation timesteps and \mathcal{S} is a set that includes SL, FL, FF, and ML. Building it requires setting a maximum number of interaction agents to prevent varying input lengths at different timesteps. If there be no interacting agent of a particular type, like i_1 (SL), at that time, its state value $x_t^{i_1}$ (x_t^{SL}) is padded to zeros. Unlike the prior interaction representation, ours can depict the target vehicle’s dynamic interactions without altering the input’s size. In Tab. 3, we additionally consider a simple agent selection method, which involves selecting the four closest neighbors within \mathcal{D} as interacting agents to demonstrate the superiority of our proposed interaction representation.

Similar to the approach of many recent studies[24, 39, 60, 25, 68], we convert the coordinate system for the final interaction representation. Specifically, all states in I are transformed into a relative coordinate system as \tilde{I} with the target vehicle’s final observation point p_0^1 as the origin and the positive direction h_0^1 of the x-axis. The conversion from absolute to relative coordinate systems significantly aids in enhancing generalization performance and reducing the learning burden, as has been validated in numerous experiments.

Interaction Modeling Our interaction encoder is primarily based on the Transformer architecture[58]. However, existing attention-based methods are purely data-driven and do not explain how the model infers the extent of correlation of inter-agent. To address this, we propose a physics-based deterministic correlation calculation method and integrate it into the Transformer.

For the traditional multi-head dot-product attention mechanism and interaction representation, the interaction embedding e_{int} between the target vehicle and all of its interaction agents can be denoted as:

$$Z = \text{FC}(\tilde{I}) = [Z^1, (Z^s)_{s \in \mathcal{S}}], \quad (4)$$

$$Q, K, V = W^q Z^1, W^k (Z^s)_{s \in \mathcal{S}}, W^v (Z^s)_{s \in \mathcal{S}}, \quad (5)$$

$$Z' = \text{MHA}(Q, K, V), \quad (6)$$

$$e_{int} = \text{LN}(\text{FFN}(\text{LN}(Z^1 + Z')) + Z), \quad (7)$$

where $\text{FC}(\cdot) \in \mathbb{R}^{7T_h \times d_z}$ performs a direct linear transformation on the temporal dimension features, and Q, K, V are obtained from three equivalent linear transformations ($W^q, W^k, W^v \in \mathbb{R}^{d_z \times d_{z'}}$). Residual connection[15] and layer normalization [1] $\text{LN}(\cdot)$ are applied to the output Z from $\text{MHA}(\cdot)$ before input into the feed-forward module $\text{FFN}(\cdot)$, following the standard Transformer architecture. It is also applicable within our proposed interaction representation.

We now introduce a physical method to calculate the correlation $\alpha_t^{i_1}$ between agent i_1 and the target vehicle at time t . First, we use the CA model to estimate the time $\tau_t^{i_1}$ needed for the target vehicle and agent i_1 to reach the closest distance $d_{t+}^{i_1}$, expressed as:

$$\tau_t^{i_1} = \arg \min_{\tau} \|\text{CA}(\tau; \tilde{x}_t^1) - \text{CA}(\tau; \tilde{x}_t^{i_1})\|_2, \quad (8)$$

$$d_{t+}^{i_1} = \|\text{CA}(\tau_t^{i_1}; \tilde{x}_t^1) - \text{CA}(\tau_t^{i_1}; \tilde{x}_t^{i_1})\|_2. \quad (9)$$

Then, combining with the current distance $d_t^{i_1}$ between them obtained from Alg. 1 to calculate the correlation coefficient :

$$\bar{\tau}_t^{i_1} = \begin{cases} 0 & \text{if } \tau_t^{i_1} < 0; \\ 30 & \text{if } \tau_t^{i_1} > 30; \\ \tau_t^{i_1} & \text{otherwise,} \end{cases} \quad (10)$$

$$c_t^{i_1} = \frac{d_t^{i_1} - d_{t+}^{i_1} + 1}{d_t^{i_1} \exp(\bar{\tau}_t^{i_1})}. \quad (11)$$

Here, we set a lower bound for $\tau_t^{i_1}$ to ensure that the correlation coefficient is based solely on future action and an upper bound based on the assumption that agents will not stay in the scene for more than 30 seconds, to prevent excessively high values in subsequent calculations. The construction of Eq. 11 is based on the correlation between agents being negatively correlated with $d_t^{i_1}$ and $\tau_t^{i_1}$ and positively correlated with the difference in the distance they cover during $\tau_t^{i_1}$. Adding one in the numerator prevents it from 0, thereby maintaining the effectiveness of the two factors in the denominator. Using $\exp(\cdot)$ in the denominator serves to highlight the impact of $\tau_t^{i_1}$ and avoid the denominator being 0. If at time t there is no SL type agent i_1 , then $c_t^{i_1}$ is naturally set to 0. Next, $c_t^{i_1}$ is normalized to a physical attention score:

$$\alpha_t^{i_1} = \alpha_t^{\text{SL}} = \frac{2(T_h + t)c_t^{i_1}}{(1 + T_h)T_h \sum_{n=1}^4 c_t^{i_n}}, \quad (12)$$

where $\alpha_t^{i_1}$ simultaneously incorporates the spatial attention of the target vehicle towards agent i_1 at time t and the linear weighting of t over the entire time scale T_h . Subsequently, we derive a weight matrix $\mathcal{A} \in \mathbb{R}^{4 \times T_h}$:

$$\mathcal{A} = \begin{bmatrix} \alpha_{-T_h+1}^{\text{SL}} & \cdots & \alpha_0^{\text{SL}} \\ \alpha_{-T_h+1}^{\text{FL}} & \cdots & \alpha_0^{\text{FL}} \\ \alpha_{-T_h+1}^{\text{FF}} & \cdots & \alpha_0^{\text{FF}} \\ \alpha_{-T_h+1}^{\text{ML}} & \cdots & \alpha_0^{\text{ML}} \end{bmatrix} = \begin{bmatrix} \mathcal{A}^{\text{SL}} \\ \mathcal{A}^{\text{FL}} \\ \mathcal{A}^{\text{FF}} \\ \mathcal{A}^{\text{ML}} \end{bmatrix}. \quad (13)$$

Ultimately, e_{int} is obtained by applying residual connection and layer norm:

$$Z = \text{FC}_z(\tilde{I}) = [Z^1, (Z^s)_{s \in \mathcal{S}}], \quad (14)$$

$$Z' = \text{FC}_{z'} \left(Z^1 + \sum_{s \in \mathcal{S}} \mathcal{A}^s \circ Z^s \right), \quad (15)$$

$$e_{int} = \text{FFN-LN}(\text{FFN}(\text{LN}(Z'))) + Z', \quad (16)$$

where $\text{FC}_z(\cdot) \in \mathbb{R}^{7 \times d_z}$ and $\text{FC}_{z'}(\cdot) \in \mathbb{R}^{d_z T_h \times d_{z'}}$ perform linear transformations on spatial and temporal features respectively, \circ denotes the Hadamard product. Inspired by NormFormer[53], we additionally use one LN placed after the FNN(\cdot) but before the residual connection on top of the Pre-LN configuration, referred to as FFN-LN(\cdot), which helps enhance training stability.

3 Experiments

Experiments are carried out on three public trajectory prediction datasets, which included comparison experiments on the INTERACTION[65] and highD[28] datasets, and ablation studies on the INTERACTION and CitySim[67] datasets. Detailed experimental setup (including datasets introduction, experimental metrics, and model implementation details) can be found in App. C. Additionally, in App. D, we compare the inference speeds of ASPILin and the baseline model to demonstrate the efficiency of our model.

3.1 Comparison with State-of-the-art

We evaluate our model on the INTERACTION and highD datasets and compare it with state-of-the-art models. ASPILin is developed in map-free and map-based versions of the INTERACTION dataset. Much recent research[60, 31, 4, 10] concentrates on map-free approaches due to the unavailability of high-definition maps, and our model can readily be adapted to a map-free model (i.e., variant 3 in Tab. 3) because each encoder operates independently. The results shown in Tab. 1 indicate that the map-free and map-based ASPILin achieve state-of-the-art performance among their respective model types. Additionally, our map-free model’s performance significantly surpasses similar models. It even achieves competitive results compared to the state-of-the-art map-based models, demonstrating the superiority of our interaction module.

The comparison results on the highD dataset are shown in Tab. 2. Similar to some work[40, 41], we first implement a Constant Velocity (CV) model as a reference baseline for the highD dataset. Interestingly, apart from the MHA-LSTM[37] and our model, all other models cannot surpass the CV model regarding predictive performance within 1 future second. The performance exhibited by Lin exceeds that of state-of-the-art methods, attributable to its superior CVAE architecture and loss functions. By comparison, ASPILin significantly lowers the RMSE after 3 future seconds, highlighting the importance of interaction modeling for long-term prediction.

3.2 Ablation Studies

A series of ablation studies are conducted to validate the advanced nature of our proposed approach on the INTERACTION and CitySim datasets, encompassing the various components of the interaction module, four types of interacting agents, and the influence of different lane predictors on the outcomes. All methods in the last two ablation experiments use our proposed interaction representation and physics-related interaction encoding method.

Table 1: Comparison with models on the INTERACTION validation set. † indicates that models do not use maps and * indicates those models that only perform unimodal predictions.

Model	minADE ₆ ↓	minFDE ₆ ↓
DESIRE[31] †	0.32	0.88
Multipath[4] †	0.30	0.99
TNT[66]	0.21	0.67
HEAT-I-R[39] *	0.19	0.66
DCM-MHA-LSTM[10] †	0.19	0.58
ITRA[50]	0.17	0.49
GOHOME[11]	-	0.45
joint-StarNet[20]	0.13	0.38
DiPA[25]	0.11	0.34
MB-SS-ASP[23]	0.10	0.30
SAN[21]	0.10	0.29
GMM-CVAE[22]	0.09	0.28
Lin † *	0.22	0.85
ASPILin †	0.12	0.43
Lin *	0.18	0.67
ASPILin	0.08	0.27

Table 2: Comparison with models on the highD test set. The best and second best results are in **bold** and underlined, respectively.

Model	RMSE↓				
	1s	2s	3s	4s	5s
CV	0.11	0.35	0.73	1.24	1.86
CS-LSTM[8]	0.19	0.57	1.16	1.96	2.96
NLS-LSTM[37]	0.22	0.61	1.24	2.10	3.27
MHA-LSTM[38]	<u>0.06</u>	0.09	0.24	0.59	1.18
PIP[54]	0.17	0.52	1.05	1.76	2.63
STDAN[5]	0.19	0.27	0.48	0.91	1.66
MMnTP[40]	0.19	0.38	0.62	0.95	1.39
POVL[41]	0.12	0.18	0.22	0.53	1.15
VVF-TP[55]	0.12	0.24	0.41	0.66	0.98
GRANP[35]	0.41	0.44	0.70	0.88	1.34
Lin	0.05	<u>0.06</u>	<u>0.11</u>	<u>0.27</u>	<u>0.54</u>
ASPILin	0.05	0.05	0.08	0.21	0.42

Table 3: Ablation experiments for each component of the interaction module

Variant	Agent Selection		Time Windows		Interaction Encoding		INTERACTION Val.		CitySim Val.	
	4 lane-related	4 closest	all	current	physics-related	attention	minADE ₆ ↓	minFDE ₆ ↓	minADE ₆ ↓	minFDE ₆ ↓
1				✓		✓	0.119	0.393	0.999	2.223
2		✓		✓		✓	0.117	0.392	1.010	2.253
3		✓	✓			✓	0.096	0.321	0.982	2.178
4	✓			✓		✓	0.097	0.331	0.973	2.164
5	✓		✓			✓	0.091	0.314	0.965	2.137
6	✓			✓	✓		0.088	0.295	0.959	2.124
7	✓		✓		✓		0.079	0.266	0.954	2.095

Components of the Interaction Module The ablation experiments for each component of the interaction module are shown in Tab 3. The baseline configuration selects all agents within \mathcal{D} at time $t = 0$ as interacting agents and encodes their interactions using two layers of Transformer. As noted earlier, we introduced an additional simple method for agent selection—selecting the four closest agents—to further verify the effectiveness of our proposed interaction representation. An intuitive conclusion is that merely setting an upper limit on the number of interaction agents does not enhance model performance and may even reduce it. This is reasonable, as inappropriately narrowing the selection range will likely exclude genuinely interacting agents. However, switching the time window from current to all results in enhanced model performance, demonstrated across all three comparison sets (variants 2 and 3, 4 and 5, 6 and 7). An interesting observation is that variants 2 and 3 are more significant than in the two other groups due to the instability of the 4 closest selection method compared to 4 lane-related. That’s because the four closest agents in interaction-dense scenarios may change at any moment, whereas four lane-related agents are less likely to change over time. From comparisons in two other groups (variants 2 and 4, 3 and 5), we conclude that refining agent selection through lane usage can improve model performance, which provides valuable insights for future research. The last two comparisons (variants 4 and 6, 5 and 7) demonstrate that our physics-based interaction encoding method is viable and advantageous, significantly increasing the model’s interpretability. Overall, our final model, compared to the baseline, shows an improvement of 33.6% in minADE₆ and 32.3% in minFDE₆ on the INTERACTION validation set and an increase of 5.5% in minADE₆ and 5.8% in minFDE₆ on the CitySim validation set.

Four Types of Interacting Agents

We conduct ablation experiments on four types of interacting agents to verify that each category positively affects model performance. According to the results in Tab. 4, excluding any category of interacting agents results in some level of decline in model performance.

Models excluding FF and FL, respectively, achieve the poorest performance on the INTERACTION and CitySim validation sets, indicating that agents on the target vehicle’s future lane have a greater impact on the target vehicle than other agents. Moreover, on the CitySim validation set, the prediction task is more sensitive to changes in interaction agents because a 6-second prediction period is more affected by interacting agents than a 3-second.

Different Lane Predictors Despite our clarification that the lane predictor based on classification is not practical for real-world applications, we implement this approach to examine how the accuracy of future lane predictions affects model performance by a simple Random Forest (RF). The detailed experimental results are

shown in Tab. 5. Using raw data undoubtedly achieves the best performance. Interestingly, the classification- and regression-based models show starkly different performances on the two datasets

Table 4: Ablation experiments for four types of interacting agents

SL	FL	FF	ML	INTERACTION Val.		CitySim Val.	
				minADE ₆ ↓	minFDE ₆ ↓	minADE ₆ ↓	minFDE ₆ ↓
	✓	✓	✓	0.083	0.282	1.013	2.235
✓		✓	✓	0.080	0.269	1.025	2.307
✓	✓		✓	0.090	0.299	1.007	2.243
✓	✓	✓		0.085	0.271	0.963	2.127
✓	✓	✓	✓	0.079	0.266	0.954	2.095

Table 5: Ablation experiments for different lane predictors

Dataset	Method	ACC(%)↑	minADE ₆ ↓	minFDE ₆ ↓
INTERACTION	Clf. (RF)	88.5	0.080	0.270
	Reg. (Lin)	97.9	0.079	0.266
	Raw Data	100	0.078	0.261
CitySim	Clf. (RF)	93.6	0.951	2.089
	Reg. (Lin)	89.5	0.954	2.095
	Raw Data	100	0.946	2.073

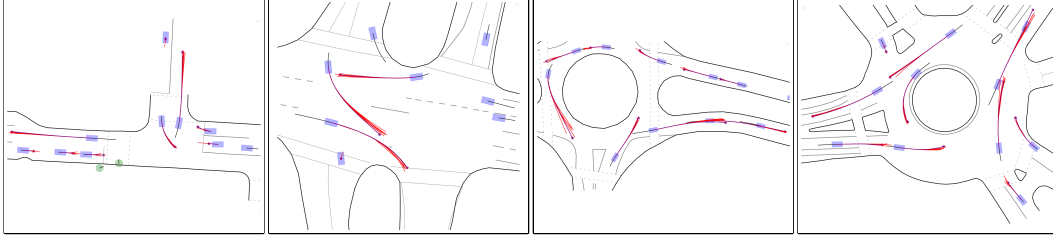


Figure 3: Qualitative results of ASPILin on the INTERACTION validation set. Purple rectangles represent vehicles, while green circles denote pedestrians or cyclists. Past trajectories are shown with black lines, predicted future trajectories with red lines, and ground-truth trajectories with purple lines, with endpoints marked distinctively.

because the prediction tasks on the CitySim dataset are considerably more complex than those on the INTERACTION, especially since interactions are not considered in both. Classification-based models can use the current lane of an agent as an additional input to simplify the prediction process, a capability that regression-based models lack. What is not displayed in the table is that Lin’s ADE and FDE on the CitySim dataset are 2.741 and 7.675, respectively. Nevertheless, it maintains a high lane prediction accuracy close to that of RF, demonstrating that our comprehensive agent selection strategy is effective even for long-term prediction tasks with a simple model. Additionally, it can be observed that different methods reduce the discrepancies in lane prediction in their final forecasts. This is because our agent selection is not entirely based on future lanes, and predicting an incorrect future lane may still lead to the same outcome due to other mismatched conditions.

3.3 Qualitative Results

We present the qualitative results of ASPILin on the INTERACTION dataset. As illustrated in Fig. 3, our model can predict accurate, multi-modal vehicle trajectories in complex scenarios. Interestingly, ASPILin struggles more with predicting the precise trajectories of vehicles that are stationary or nearly so, as they have less dynamic information and greater randomness. This observation also points to potential areas for future enhancements.

4 Limitations

While the experiments showcase our proposed methods’ excellent performance, they still have limitations. In App. E, we elaborate on these limitations, covering the limitations of ASPILin and the limitations of the three enhancement methods we proposed for the interaction module.

5 Conclusions

In this work, we explored the possibility of enhancing single-agent trajectory prediction interaction from multiple perspectives, including (i) a lane-related method for a more detailed selection of interacting agents, (ii) a simple interaction representation that captures dynamic interactions, and (iii) a physically-related interaction encoding method. We designed a model named ASPILin and conducted experiments on the INTERACTION, highD, and CitySim datasets. The results indicate that our approach significantly enhances interaction modeling and positively affects trajectory prediction, offering substantially increased interpretability over earlier methods. Furthermore, our proposed interaction components can be readily integrated into other model architectures due to their independence.

One future work area involves modeling more high-level interactions, benefiting multi-agent and one-shot long-term predictions. Another promising direction is to explore more possibilities of combining data-driven and physical methods, further enhancing the model’s interpretability and generalizability.

References

- [1] Jimmy Ba, Jamie Ryan Kiros, and Geoffrey E. Hinton. Layer normalization. *ArXiv*, abs/1607.06450, 2016. URL <https://api.semanticscholar.org/CorpusID:8236317>.
- [2] Prarthana Bhattacharyya, Chengjie Huang, and K. Czarnecki. Ssl-lanes: Self-supervised learning for motion forecasting in autonomous driving. *ArXiv*, abs/2206.14116, 2022. URL <https://api.semanticscholar.org/CorpusID:250089044>.
- [3] Sergio Casas, Cole Gulino, Simon Suo, Katie Luo, Renjie Liao, and Raquel Urtasun. Implicit latent variable model for scene-consistent motion forecasting. *ArXiv*, abs/2007.12036, 2020. URL <https://api.semanticscholar.org/CorpusID:220713282>.
- [4] Yuning Chai, Benjamin Sapp, Mayank Bansal, and Dragomir Anguelov. Multipath: Multiple probabilistic anchor trajectory hypotheses for behavior prediction. In *Conference on Robot Learning*, 2019. URL <https://api.semanticscholar.org/CorpusID:204509212>.
- [5] Xiaobo Chen, Huanjian Zhang, Fengyin Zhao, Yu Hu, Chenkai Tan, and Jian Yang. Intention-aware vehicle trajectory prediction based on spatial-temporal dynamic attention network for internet of vehicles. *IEEE Transactions on Intelligent Transportation Systems*, 23:19471–19483, 2022. URL <https://api.semanticscholar.org/CorpusID:248548325>.
- [6] Alexander Cui, Abbas Sadat, Sergio Casas, Renjie Liao, and Raquel Urtasun. Lookout: Diverse multi-future prediction and planning for self-driving. *2021 IEEE/CVF International Conference on Computer Vision (ICCV)*, pages 16087–16096, 2021. URL <https://api.semanticscholar.org/CorpusID:231632845>.
- [7] Henggang Cui, Vladan Radosavljevic, Fang-Chieh Chou, Tsung-Han Lin, Thi Nguyen, Tzu-Kuo Huang, Jeff G. Schneider, and Nemanja Djuric. Multimodal trajectory predictions for autonomous driving using deep convolutional networks. *2019 International Conference on Robotics and Automation (ICRA)*, pages 2090–2096, 2018. URL <https://api.semanticscholar.org/CorpusID:52891221>.
- [8] Nachiket Deo and Mohan Manubhai Trivedi. Convolutional social pooling for vehicle trajectory prediction. *2018 IEEE/CVF Conference on Computer Vision and Pattern Recognition Workshops (CVPRW)*, pages 1549–15498, 2018. URL <https://api.semanticscholar.org/CorpusID:21712887>.
- [9] Jiyang Gao, Chen Sun, Hang Zhao, Yi Shen, Dragomir Anguelov, Congcong Li, and Cordelia Schmid. Vectornet: Encoding hd maps and agent dynamics from vectorized representation. *2020 IEEE/CVF Conference on Computer Vision and Pattern Recognition (CVPR)*, pages 11522–11530, 2020. URL <https://api.semanticscholar.org/CorpusID:218581144>.
- [10] Amina Ghoul, Itheri Yahiaoui, Anne Verroust-Blondet, and Fawzi Nashashibi. Interpretable goal-based model for vehicle trajectory prediction in interactive scenarios. *2023 IEEE Intelligent Vehicles Symposium (IV)*, pages 1–6, 2023. URL <https://api.semanticscholar.org/CorpusID:260255262>.
- [11] Thomas Gilles, Stefano Sabatini, Dzmitry V. Tsishkou, Bogdan Stanculescu, and Fabien Moutarde. Gohome: Graph-oriented heatmap output for future motion estimation. *2022 International Conference on Robotics and Automation (ICRA)*, pages 9107–9114, 2021. URL <https://api.semanticscholar.org/CorpusID:237263205>.
- [12] Tianpei Gu, Guangyi Chen, Junlong Li, Chunze Lin, Yongming Rao, Jie Zhou, and Jiwen Lu. Stochastic trajectory prediction via motion indeterminacy diffusion. *2022 IEEE/CVF Conference on Computer Vision and Pattern Recognition (CVPR)*, pages 17092–17101, 2022. URL <https://api.semanticscholar.org/CorpusID:247748591>.
- [13] Agrim Gupta, Justin Johnson, Li Fei-Fei, Silvio Savarese, and Alexandre Alahi. Social gan: Socially acceptable trajectories with generative adversarial networks. In *2018 IEEE/CVF Conference on Computer Vision and Pattern Recognition*, pages 2255–2264, 2018. doi: 10.1109/CVPR.2018.00240.
- [14] Ganglei He, Xin Li, Ying Lv, Bingzhao Gao, and Hong Chen. Probabilistic intention prediction and trajectory generation based on dynamic bayesian networks. In *2019 Chinese Automation Congress (CAC)*, pages 2646–2651, 2019. doi: 10.1109/CAC48633.2019.8996494.
- [15] Kaiming He, X. Zhang, Shaoqing Ren, and Jian Sun. Deep residual learning for image recognition. *2016 IEEE Conference on Computer Vision and Pattern Recognition (CVPR)*, pages 770–778, 2015. URL <https://api.semanticscholar.org/CorpusID:206594692>.

- [16] Yanjun Huang, Jiatong Du, Ziru Yang, Zewei Zhou, Lin Zhang, and Hong Chen. A survey on trajectory-prediction methods for autonomous driving. *IEEE Transactions on Intelligent Vehicles*, 7(3):652–674, 2022. doi: 10.1109/TIV.2022.3167103.
- [17] Yanjun Huang, Jiatong Du, Ziru Yang, Zewei Zhou, Lin Zhang, and Hong Chen. A survey on trajectory-prediction methods for autonomous driving. *IEEE Transactions on Intelligent Vehicles*, 7:652–674, 2022. URL <https://api.semanticscholar.org/CorpusID:248174848>.
- [18] Zhiyu Huang, Xiaoyu Mo, and Chen Lv. Multi-modal motion prediction with transformer-based neural network for autonomous driving. *2022 International Conference on Robotics and Automation (ICRA)*, pages 2605–2611, 2021. URL <https://api.semanticscholar.org/CorpusID:237503713>.
- [19] Faris Janjos, Maxim Dolgov, and Johann Marius Zöllner. Self-supervised action-space prediction for automated driving. *2021 IEEE Intelligent Vehicles Symposium (IV)*, pages 200–207, 2021. URL <https://api.semanticscholar.org/CorpusID:237581510>.
- [20] Faris Janjos, Maxim Dolgov, and Johann Marius Zöllner. Starnet: Joint action-space prediction with star graphs and implicit global-frame self-attention. *2022 IEEE Intelligent Vehicles Symposium (IV)*, pages 280–286, 2021. URL <https://api.semanticscholar.org/CorpusID:244708950>.
- [21] Faris Janjos, Maxim Dolgov, Muhamed Kuric, Yinzhe Shen, and Johann Marius Zöllner. San: Scene anchor networks for joint action-space prediction. *2022 IEEE Intelligent Vehicles Symposium (IV)*, pages 1751–1756, 2022. URL <https://api.semanticscholar.org/CorpusID:250721216>.
- [22] Faris Janjos, Marcel Hallgarten, Anthony Knittel, Maxim Dolgov, Andreas Zell, and Johann Marius Zöllner. Conditional unscented autoencoders for trajectory prediction. *ArXiv*, abs/2310.19944, 2023. URL <https://api.semanticscholar.org/CorpusID:264828890>.
- [23] Faris Janjos, Max Keller, Maxim Dolgov, and Johann Marius Zöllner. Bridging the gap between multi-step and one-shot trajectory prediction via self-supervision. *2023 IEEE Intelligent Vehicles Symposium (IV)*, pages 1–8, 2023. URL <https://api.semanticscholar.org/CorpusID:259088972>.
- [24] Xiaosong Jia, Peng Wu, Li Chen, Hongyang Li, Yu Sen Liu, and Junchi Yan. Hdgt: Heterogeneous driving graph transformer for multi-agent trajectory prediction via scene encoding. *IEEE Transactions on Pattern Analysis and Machine Intelligence*, 45:13860–13875, 2022. URL <https://api.semanticscholar.org/CorpusID:248965065>.
- [25] Anthony Knittel, Majd Hawasly, Stefano V. Albrecht, John Redford, and Subramanian Ramamoorthy. Dipa: Probabilistic multi-modal interactive prediction for autonomous driving. *IEEE Robotics and Automation Letters*, 8:4887–4894, 2022. URL <https://api.semanticscholar.org/CorpusID:257405440>.
- [26] Vineet Kosaraju, Amir Sadeghian, Roberto Martín-Martín, Ian Reid, S. Hamid Rezatofighi, and Silvio Savarese. Social-bigat: Multimodal trajectory forecasting using bicycle-gan and graph attention networks, 2019.
- [27] Youssef Kossale, Mohammed Airaj, and Aziz Darouichi. Mode collapse in generative adversarial networks: An overview. *2022 8th International Conference on Optimization and Applications (ICOA)*, pages 1–6, 2022. URL <https://api.semanticscholar.org/CorpusID:253425101>.
- [28] Robert Krajewski, Julian Bock, Laurent Kloeker, and Lutz Eckstein. The highd dataset: A drone dataset of naturalistic vehicle trajectories on german highways for validation of highly automated driving systems. *2018 21st International Conference on Intelligent Transportation Systems (ITSC)*, pages 2118–2125, 2018. URL <https://api.semanticscholar.org/CorpusID:53115284>.
- [29] Puneet Kumar, Mathias Perrollaz, Stéphanie Lefèvre, and Christian Laugier. Learning-based approach for online lane change intention prediction. In *2013 IEEE Intelligent Vehicles Symposium (IV)*, pages 797–802, 2013. doi: 10.1109/IVS.2013.6629564.
- [30] Namhoon Lee, Wongun Choi, Paul Vernaza, Christopher B. Choy, Philip H. S. Torr, and Manmohan Chandraker. Desire: Distant future prediction in dynamic scenes with interacting agents. In *2017 IEEE Conference on Computer Vision and Pattern Recognition (CVPR)*, pages 2165–2174, 2017. doi: 10.1109/CVPR.2017.233.
- [31] Namhoon Lee, Wongun Choi, Paul Vernaza, Christopher Bongsoo Choy, Philip H. S. Torr, and Manmohan Chandraker. Desire: Distant future prediction in dynamic scenes with interacting agents. *2017 IEEE Conference on Computer Vision and Pattern Recognition (CVPR)*, pages 2165–2174, 2017. URL <https://api.semanticscholar.org/CorpusID:8394584>.

- [32] Mengmeng Liu, Hao Cheng, Linyuan Chen, Hellward Broszio, Jiangtao Li, Runjiang Zhao, Monika Sester, and Michael Ying Yang. Laformer: Trajectory prediction for autonomous driving with lane-aware scene constraints. *ArXiv*, abs/2302.13933, 2023. URL <https://api.semanticscholar.org/CorpusID:257219389>.
- [33] Yicheng Liu, Jinghui Zhang, Liangji Fang, Qinrong Jiang, and Bolei Zhou. Multimodal motion prediction with stacked transformers. *2021 IEEE/CVF Conference on Computer Vision and Pattern Recognition (CVPR)*, pages 7573–7582, 2021. URL <https://api.semanticscholar.org/CorpusID:232307829>.
- [34] Ilya Loshchilov and Frank Hutter. Sgdr: Stochastic gradient descent with warm restarts. *arXiv: Learning*, 2016. URL <https://api.semanticscholar.org/CorpusID:14337532>.
- [35] Yuhao Luo, Kehua Chen, and Meixin Zhu. Granp: A graph recurrent attentive neural process model for vehicle trajectory prediction. 2024. URL <https://api.semanticscholar.org/CorpusID:269137536>.
- [36] Wei Mao, Chenxin Xu, Qi Zhu, Siheng Chen, and Yanfeng Wang. Leapfrog diffusion model for stochastic trajectory prediction. *2023 IEEE/CVF Conference on Computer Vision and Pattern Recognition (CVPR)*, pages 5517–5526, 2023. URL <https://api.semanticscholar.org/CorpusID:257631504>.
- [37] Kaouther Messaoud, Itheri Yahiaoui, Anne Verroust-Blondet, and Fawzi Nashashibi. Non-local social pooling for vehicle trajectory prediction. *2019 IEEE Intelligent Vehicles Symposium (IV)*, pages 975–980, 2019. URL <https://api.semanticscholar.org/CorpusID:198311952>.
- [38] Kaouther Messaoud, Itheri Yahiaoui, Anne Verroust-Blondet, and Fawzi Nashashibi. Attention based vehicle trajectory prediction. *IEEE Transactions on Intelligent Vehicles*, 6:175–185, 2020. URL <https://api.semanticscholar.org/CorpusID:218794246>.
- [39] Xiaoyu Mo, Zhiyu Huang, Yang Xing, and Chen Lv. Multi-agent trajectory prediction with heterogeneous edge-enhanced graph attention network. *IEEE Transactions on Intelligent Transportation Systems*, 23: 9554–9567, 2022. URL <https://api.semanticscholar.org/CorpusID:246551264>.
- [40] Sajjad Mozaffari, Mreza Alipour Sormoli, Konstantinos Koufos, and Mehrdad Dianati. Multimodal manoeuvre and trajectory prediction for automated driving on highways using transformer networks. *IEEE Robotics and Automation Letters*, 8:6123–6130, 2023. URL <https://api.semanticscholar.org/CorpusID:260164486>.
- [41] Sajjad Mozaffari, Mreza Alipour Sormoli, Konstantinos Koufos, Graham Lee, and Mehrdad Dianati. Trajectory prediction with observations of variable-length for motion planning in highway merging scenarios. *2023 IEEE 26th International Conference on Intelligent Transportation Systems (ITSC)*, pages 5633–5640, 2023. URL <https://api.semanticscholar.org/CorpusID:259129539>.
- [42] Jiquan Ngiam, Vijay Vasudevan, Benjamin Caine, Zhengdong Zhang, Hao-Tien Lewis Chiang, Jeffrey Ling, Rebecca Roelofs, Alex Bewley, Chenxi Liu, Ashish Venugopal, David J. Weiss, Benjamin Sapp, Zhifeng Chen, and Jonathon Shlens. Scene transformer: A unified architecture for predicting future trajectories of multiple agents. In *International Conference on Learning Representations*, 2022. URL <https://api.semanticscholar.org/CorpusID:251648671>.
- [43] Seong Hyeon Park, ByeongDo Kim, Chang Mook Kang, Chung Choo Chung, and Jun Won Choi. Sequence-to-sequence prediction of vehicle trajectory via lstm encoder-decoder architecture. In *2018 IEEE Intelligent Vehicles Symposium (IV)*, pages 1672–1678, 2018. doi: 10.1109/IVS.2018.8500658.
- [44] Shan Bao Ruifeng Zhang, Libo Cao and Jianjie Tan. A method for connected vehicle trajectory prediction and collision warning algorithm based on v2v communication. *International Journal of Crashworthiness*, 22(1):15–25, 2017. doi: 10.1080/13588265.2016.1215584. URL <https://doi.org/10.1080/13588265.2016.1215584>.
- [45] Amir Sadeghian, Vineet Kosaraju, Ali Sadeghian, Noriaki Hirose, Hamid Rezatofghi, and Silvio Savarese. Sophie: An attentive gan for predicting paths compliant to social and physical constraints. In *2019 IEEE/CVF Conference on Computer Vision and Pattern Recognition (CVPR)*, pages 1349–1358, 2019. doi: 10.1109/CVPR.2019.00144.
- [46] Tim Salzmann, B. Ivanovic, Punarjay Chakravarty, and Marco Pavone. Trajectron++: Dynamically-feasible trajectory forecasting with heterogeneous data. In *European Conference on Computer Vision*, 2020. URL <https://api.semanticscholar.org/CorpusID:214802528>.
- [47] Tim Salzmann, B. Ivanovic, Punarjay Chakravarty, and Marco Pavone. Trajectron++: Multi-agent generative trajectory forecasting with heterogeneous data for control. *ArXiv*, abs/2001.03093, 2020. URL <https://api.semanticscholar.org/CorpusID:210116551>.

- [48] Tim Salzmann, Boris Ivanovic, Punarjay Chakravarty, and Marco Pavone. Trajectron++: Dynamically-feasible trajectory forecasting with heterogeneous data. In Andrea Vedaldi, Horst Bischof, Thomas Brox, and Jan-Michael Frahm, editors, *Computer Vision – ECCV 2020*, pages 683–700, Cham, 2020. Springer International Publishing. ISBN 978-3-030-58523-5.
- [49] Jens Schulz, Constantin Hubmann, Julian Löchner, and Darius Burschka. Interaction-aware probabilistic behavior prediction in urban environments. *2018 IEEE/RSJ International Conference on Intelligent Robots and Systems (IROS)*, pages 3999–4006, 2018. URL <https://api.semanticscholar.org/CorpusID:13739957>.
- [50] Adam Scibior, Vasileios Lioutas, Daniele Reda, Peyman Bateni, and Frank D. Wood. Imagining the road ahead: Multi-agent trajectory prediction via differentiable simulation. *2021 IEEE International Intelligent Transportation Systems Conference (ITSC)*, pages 720–725, 2021. URL <https://api.semanticscholar.org/CorpusID:233347183>.
- [51] Chengchao Shen, Youtan Yin, Xinchao Wang, Xubin Li, Jie Song, and Mingli Song. Training generative adversarial networks in one stage. *2021 IEEE/CVF Conference on Computer Vision and Pattern Recognition (CVPR)*, pages 3349–3359, 2021. URL <https://api.semanticscholar.org/CorpusID:232075932>.
- [52] Shaoshuai Shi, Li Jiang, Dengxin Dai, and Bernt Schiele. Mtr++: Multi-agent motion prediction with symmetric scene modeling and guided intention querying. *IEEE transactions on pattern analysis and machine intelligence*, PP, 2023. URL <https://api.semanticscholar.org/CorpusID:259308934>.
- [53] Sam Shleifer, Jason Weston, and Myle Ott. Normformer: Improved transformer pretraining with extra normalization. *ArXiv*, abs/2110.09456, 2021. URL <https://api.semanticscholar.org/CorpusID:239016890>.
- [54] Haoran Song, Wenchao Ding, Yuxuan Chen, Shaojie Shen, Michael Yu Wang, and Qifeng Chen. Pip: Planning-informed trajectory prediction for autonomous driving. In *European Conference on Computer Vision*, 2020. URL <https://api.semanticscholar.org/CorpusID:214641168>.
- [55] Mreza Alipour Sormoli, Amir Samadi, Sajjad Mozaffari, Konstantinos Koufos, Mehrdad Dianati, and Roger Woodman. A novel deep neural network for trajectory prediction in automated vehicles using velocity vector field. *2023 IEEE 26th International Conference on Intelligent Transportation Systems (ITSC)*, pages 4003–4010, 2023. URL <https://api.semanticscholar.org/CorpusID:261974973>.
- [56] Qiao Sun, Xin Huang, Junru Gu, Brian Charles Williams, and Hang Zhao. M2i: From factored marginal trajectory prediction to interactive prediction. *2022 IEEE/CVF Conference on Computer Vision and Pattern Recognition (CVPR)*, pages 6533–6542, 2022. URL <https://api.semanticscholar.org/CorpusID:247083998>.
- [57] Balakrishnan Varadarajan, Ahmed S. Hefny, Avikalp Srivastava, Khaled S. Refaat, Nigamaa Nayakanti, Andre Comman, K. M. Chen, Bertrand Douillard, C. P. Lam, Drago Anguelov, and Benjamin Sapp. Multipath++: Efficient information fusion and trajectory aggregation for behavior prediction. *2022 International Conference on Robotics and Automation (ICRA)*, pages 7814–7821, 2021. URL <https://api.semanticscholar.org/CorpusID:244730940>.
- [58] Ashish Vaswani, Noam M. Shazeer, Niki Parmar, Jakob Uszkoreit, Llion Jones, Aidan N. Gomez, Lukasz Kaiser, and Illia Polosukhin. Attention is all you need. In *Neural Information Processing Systems*, 2017. URL <https://api.semanticscholar.org/CorpusID:13756489>.
- [59] Yuting Wang, Hangning Zhou, Zhigang Zhang, Chen Feng, Huan-Yu Lin, Chaofei Gao, Yizhi Tang, Zhenting Zhao, Shiyu Zhang, Jie Guo, Xuefeng Wang, Ziyao Xu, and Chi Zhang. Tenet: Transformer encoding network for effective temporal flow on motion prediction. *ArXiv*, abs/2207.00170, 2022. URL <https://api.semanticscholar.org/CorpusID:250243732>.
- [60] Junhong Xiang, Zhixiong Nan, Zhe Song, Jun Huang, and Lingxi Li. Map-free trajectory prediction in traffic with multi-level spatial-temporal modeling. *IEEE Transactions on Intelligent Vehicles*, pages 1–13, 2023. doi: 10.1109/TIV.2023.3342430.
- [61] Junhong Xiang, Zhixiong Nan, Zhe Song, Jun Huang, and Lingxi Li. Map-free trajectory prediction in traffic with multi-level spatial-temporal modeling. *IEEE Transactions on Intelligent Vehicles*, 2023. URL <https://api.semanticscholar.org/CorpusID:266303007>.
- [62] Guotao Xie, Hongbo Gao, Lijun Qian, Bin Huang, Keqiang Li, and Jianqiang Wang. Vehicle trajectory prediction by integrating physics- and maneuver-based approaches using interactive multiple models. *IEEE Transactions on Industrial Electronics*, 65:5999–6008, 2018. URL <https://api.semanticscholar.org/CorpusID:3784884>.

- [63] Dongwei Xu, Xuettian Shang, Yewanze Liu, Hang Peng, and Haijian Li. Group vehicle trajectory prediction with global spatio-temporal graph. *IEEE Transactions on Intelligent Vehicles*, 8:1219–1229, 2023. URL <https://api.semanticscholar.org/CorpusID:251755175>.
- [64] Ye Yuan, Xinshuo Weng, Yanglan Ou, and Kris Kitani. Agentformer: Agent-aware transformers for socio-temporal multi-agent forecasting. *2021 IEEE/CVF International Conference on Computer Vision (ICCV)*, pages 9793–9803, 2021. URL <https://api.semanticscholar.org/CorpusID:232352504>.
- [65] Wei Zhan, Liting Sun, Di Wang, Haojie Shi, Aubrey Clausse, Maximilian Naumann, Julius Kümmerle, Hendrik Königshof, Christoph Stiller, Arnaud de La Fortelle, and Masayoshi Tomizuka. Interaction dataset: An international, adversarial and cooperative motion dataset in interactive driving scenarios with semantic maps. *ArXiv*, abs/1910.03088, 2019. URL <https://api.semanticscholar.org/CorpusID:203902759>.
- [66] Hang Zhao, Jiyang Gao, Tian Lan, Chen Sun, Benjamin Sapp, Balakrishnan Varadarajan, Yue Shen, Yi Shen, Yuning Chai, Cordelia Schmid, Congcong Li, and Dragomir Anguelov. Tnt: Target-driven trajectory prediction. In *Conference on Robot Learning*, 2020. URL <https://api.semanticscholar.org/CorpusID:221172860>.
- [67] Ou Zheng, Mohamed A. Abdel-Aty, Lishengsa Yue, Amr Abdelraouf, Zijin Wang, and Nada Mahmoud. Citysim: A drone-based vehicle trajectory dataset for safety oriented research and digital twins. *ArXiv*, abs/2208.11036, 2022. URL <https://api.semanticscholar.org/CorpusID:251741516>.
- [68] Zikang Zhou, Luyao Ye, Jianping Wang, Kui Wu, and Kejie Lu. Hivt: Hierarchical vector transformer for multi-agent motion prediction. *2022 IEEE/CVF Conference on Computer Vision and Pattern Recognition (CVPR)*, pages 8813–8823, 2022. URL <https://api.semanticscholar.org/CorpusID:250602571>.

A Related Work

A.1 Interaction-Aware Trajectory Prediction

Due to the importance of inter-agent interaction in trajectory prediction, many deep learning methods in the past have focused on modeling interactions between agents. We focus on their range of interacting agent selection, interaction time window, methods of encoding interactions, and prediction mode. Tab. 6 summarizes previous work, where models[21, 22, 66] using the same encoding interactions method are placed on the same row. Here, we perform a more meticulous analysis.

Table 6: A survey of previous work in interaction modeling

Method	Agent Selection	Time Windows	Interaction Encoding	Mode
VectorNet[9, 66]	within 130×130m	all timesteps	attention	one-shot
Agentformer[64]	within 100m	current timestep	attention	multi-step
ITRA[50]	within 100×100m	all timesteps	conv	multi-step
mmTransformer[33]	all agents	current timestep	attention	one-shot
MultiModalTransformer[18]	within 30m and up to 10 neighbors	current timestep	attention	one-shot
GOHOME[11]	within 128×128m	current timestep	attention	one-shot
MultiPath++[57]	within 80m	current timestep	RNNs	one-shot
StarNet[20–22]	within a certain threshold	current timestep	attention	one-shot
HEAT-I-R[39]	within 30m	current timestep	attention	one-shot
HiVTI[68]	within 50m	all timesteps	attention	one-shot
HDGT[24]	within 30m/20m/10m	current timestep	attention	one-shot
DiPA[25]	within 13×3 grid	current timestep	GNN	one-shot
SSL-Lanes[2]	within 100m	current timestep	attention	one-shot
SceneTransformer[42]	all agents	current timestep	attention	one-shot
TENET[59]	within 100m	current timestep	attention	one-shot
M2I[56]	all agents	current timestep	GNN+attention+physics-related	one-shot
LAformer[32]	all agents	current timestep	attention	one-shot
MTR++[52]	up to 16 neighbors	current timestep	attention	one-shot
ASPILin	up to 4 well-chosen neighbors	all timesteps	physics-related attention	one-shot

Interacting Agent Selection Methods[33, 42, 32] such as mmTransformer directly model interactions with all agents within the scene and simultaneously predict the trajectories of multiple target vehicles. While using a relative coordinate system can distinguish the context of different target vehicles, this approach still significantly increases the complexity of the model. By contrast, setting a range threshold[9, 64, 50, 18, 11, 57, 20, 39, 24, 25, 2, 59] or limiting the maximum number[18, 52] of neighbors permits modeling of the target vehicle’s local context, which aligns more closely with the needs of single-agent prediction[9, 18, 11, 20]. Moreover, many works[20, 52, 68] conduct joint predictions by initially capturing local interactions before modeling global interactions, enabling the model to extend from single-agent prediction to multi-agent prediction. Nonetheless, their selection mechanisms are still too simplistic, especially in scenarios with dense agent populations where the agents truly interacting might represent a very small fraction. In this work, we use the future lane of each agent as its intention further to select the interacting agents for the target vehicle.

Interaction Time Windows Many methods only model the relationship between the target vehicle and the interacting agents selected at the current time, potentially leading the model to ignore dynamic interactions over time. Because in the early stages of observation, the target vehicle may not interact with these agents. While employing a broader range for agent selection might somewhat mitigate this issue, as noted earlier, it considerably lowers modeling efficiency. Hence, we propose to select interacting agents for each timestep and only extract their features at that timestep, thereby capturing dynamic interactions without enlarging the input size. Additionally, differing from other models that follow the same methodology, we neither adopt a multi-step prediction strategy[50] nor utilize vectorized input representations for separate modeling[9, 68]. Conversely, we model the entire point-based input in one go and directly predict the trajectories for all future timesteps.

Interaction Encoding Almost all work uses purely data-driven approaches. However, recent studies indicate that incorporating physics can enhance the performance of deep learning models. SSP-ASP[19] and ITRA[50] purely limit motion learning to an action space grounded in acceleration and steering angles, subsequently deducing future trajectories via a kinematic model. M2I[56] classifies a pair of agents as influencer and reactor by calculating the closest value of their ground-truth trajectories and the time required to reach the nearest point at the training stage, followed by the sequential generation of their future trajectories via a marginal predictor and a conditional predictor, respectively. Differently, through a physical model, we estimate the nearest future distance between

agents and the time needed to reach this distance, integrating these with their current distance to compute a physical correlation coefficient.

A.2 Multi-modal Trajectory Prediction

The future trajectory of vehicles inherently exhibits multimodality, given the uncertainty of intentions. Early approaches are commonly based on deterministic methods from physics or classic machine learning, such as Kalman Filtering (KF)[44], Dynamic Bayesian Network (DBN)[14], Support Vector Machines (SVM)[29], etc.

To tackle this challenge, one widely used approach involves modeling the output as a probability distribution of future trajectories via regression[7, 61]. Usually, it introduces a cross-entropy loss function for mode classification to avoid mode collapse. Additionally, some methods[66, 2] use more explicit classification representations to make multi-modal trajectories closer to reality. TNT[66] samples anchor points from the roadmap and then generates trajectories based on these anchors. SSL-Lanes[2] classifies the maneuvers of each agent and trains the model in a self-supervised manner.

Other methods parameterize the distribution of future trajectories[57, 47], such as Gaussian Mixture Models (GMM) or samples within a latent space and generate predictions through mapping. Regarding the latter, Generative Adversarial Networks (GANs)[13, 45, 26] and Conditional Variational Autoencoders (CVAEs)[48, 30, 43] are the most popular models. A common drawback of generative models is the need for extensive data to support training. Moreover, for GANs, challenges such as training difficulties[51] and mode collapse[27] exist. Although CVAEs face similar issues of insufficient diversity, their training is more stable. In this study, we employ a reparameterized architecture to predict future vehicle trajectories. Instead of sampling randomly from a standard normal distribution, we treat the sampler as a trainable module to prevent unrealistic trajectory outputs due to randomness.

B More Details of ASPILin

B.1 Other Crucial Modules

For other model components, we use the prototype components of leapfrog[36] (excluding the map encoder). They all consist of simple neural networks, improving the efficiency of model inference and highlighting the advantages of our interaction module.

Spatiotemporal Encoder 1D Convolutional Neural Networks $\text{Conv1D}(\cdot)$ and Gated Recurrent Units $\text{GRU}(\cdot)$ are used to capture the spatial and temporal dependencies of the target vehicle’s historical states in the relative coordinate system, ultimately resulting in a spatiotemporal embedding e_{st} :

$$e_{st} = \text{GRU}(\text{Conv1D}(\{\tilde{x}_k^1\}_{k=-T_h+1}^0)). \quad (17)$$

We use three equivalent but independent spatiotemporal encoders corresponding to decoders to obtain the mean μ , variance σ , and samples z used for reparameterization respectively. The corresponding embeddings are labeled as e_{st}^μ , e_{st}^σ , and e_{st}^z .

Map Encoder The map selector from HEAT-I-R[39] is utilized as our map encoder, employing a gating mechanism on map features extracted by CNN for selecting maps. This enables agents in varying states to pay attention to specific map features, rather than sharing a single global map or storing a local map for each agent. The entire process is as follows:

$$\mathcal{M}' = \text{MLP}(\text{CNNs}(\mathcal{M})), \quad (18)$$

$$x' = \text{FC}_{x'}(x_0^1), \quad (19)$$

$$e_{map} = \text{Sigmoid}(\text{FC}_m([\mathcal{M}', x'])) \circ \mathcal{M}'. \quad (20)$$

More precisely, we initially utilize $\text{CNNs}(\cdot)$ and $\text{MLP}(\cdot)$ to extract features from the map and perform a linear transformation ($\text{FC}_{x'}(\cdot) \in \mathbb{R}^{7 \times d_{x'}}$) of the target agent’s state at the current time from global coordinates into a higher-dimensional space. Then, we fuse the features of x' and \mathcal{M}' ($\text{FC}_m(\cdot) \in \mathbb{R}^{(d_{x'} + d_{\mathcal{M}'}) \times d_{\mathcal{M}'}}$), pass them through $\text{Sigmoid}(\cdot)$ to scale all feature values between 0 and 1, and finally perform element-wise production with \mathcal{M}' to obtain the map embedding e_{map} .

Decoder and Reparameterization We employ three distinct MLPs to serve as decoders corresponding to three spatiotemporal encoders; however, we initially forecast the mean and variance of the

future trajectory of the target vehicle, denoted as:

$$\mu = \text{MLP}_\mu([e_{st}^\mu, e_{int}, e_{map}]) = [\mu_1, \mu_2, \dots, \mu_{T_f}], \quad (21)$$

$$\sigma = \text{MLP}_\sigma([e_{st}^\sigma, e_{int}, e_{map}]), \quad (22)$$

where $\mu \in \mathbb{R}^{T_f \times 2}$ represents a set containing the means of the trajectory for each future timestep, whereas $\sigma \in \mathbb{R}$ is a single value. Next, we perform a set of linear transformations on the predicted σ and use it for sample prediction:

$$\sigma' = \text{MLP}_{\sigma'}(\sigma), \quad (23)$$

$$z = \text{MLP}_z([e_{st}^z, e_{int}, e_{map}, \sigma']) = [\{z_t^1\}_{t=1}^{T_f}, \dots, \{z_t^K\}_{t=1}^{T_f}], \quad (24)$$

where $z \in \mathbb{R}^{K \times T_f \times 2}$ represents the K samples for each future timestep. The predicted trajectory \hat{Y} is ultimately derived from a reparameterization formula:

$$\hat{Y} = \mu + \sigma \times z. \quad (25)$$

B.2 Training Objective

The loss function used to optimize both ASPILin and Lin is expressed as:

$$\mathcal{L} = \mathcal{L}_{\text{distance}} + \lambda \mathcal{L}_{\text{diversity}}, \quad (26)$$

$$\mathcal{L}_{\text{distance}} = \frac{1}{T_f} \min_{k=1}^K \sum_{t=1}^{T_f} \|\hat{y}_t^k - y_t\|_2, \quad (27)$$

$$\mathcal{L}_{\text{diversity}} = \frac{\sum_{k=1}^K \sum_{t=1}^{T_f} \|\hat{y}_t^k - y_t\|_2}{\sigma^2 K T_f} + \log \sigma^2. \quad (28)$$

We apply a winner-takes-all strategy to $\mathcal{L}_{\text{distance}}$, performing backpropagation only on the mode with the smallest deviation from the ground-truth to prevent mode collapse. $\mathcal{L}_{\text{diversity}}$ with $\lambda = 0.02$ is designed to enhance the diversity of forecasted trajectories. The first component aligns variance with scene complexity, while the second component acts as a regularization factor, ensuring high variance across all predictions.

C Experimental Setup

C.1 Datasets

The INTERACTION dataset[65] primarily focuses on interactions between agents, including trajectories of vehicles and pedestrians or cyclists in intersections, roundabouts, and merging scenarios across multiple countries. All these no-signal scenarios are recorded at a trajectory sampling rate of 10Hz, with the task being to predict the trajectory of the next 3 seconds (30 timesteps) based on the previous 1 second (10 timesteps). We use the officially divided training set and validation set, training and evaluating ASPILin using only vehicle trajectories, including 398,409 training sequences and 107,269 validation sequences. For Lin, we train using trajectories from all agent types, including 413,548 training sequences and 111,493 validation sequences.

The highD dataset[28] is centered on highway vehicle trajectories, specifically focusing on interactions such as lane changing and overtaking. The sampling rate for trajectories is 25Hz. To fairly compare with the state-of-the-art methods, we split the dataset into training, validation, and test sets in a 7:1:2 ratio and downsample the trajectories to 5Hz, following the data processing steps in PiP[54]. The prediction task involves using the past 3 seconds (15 timesteps) to predict the next 5 seconds (25 timesteps). ASPILin and Lin use the same data for training and inference, including 2,530,166 training sequences and 361,454 test sequences.

The CitySim dataset[67], launched in 2023, is designed to advance safety-oriented research, providing more precise trajectories and more labels and increased numbers of interaction safety incidents than previous datasets. We use data from two unsignalized scenarios, Intersection B and Roundabout A, for training and evaluating the model, with the training and validation split in an 8:2 ratio. The trajectory sampling rate for both scenarios is 30Hz, with the task being to predict the future 6s (180 timesteps) trajectory based on the past 2s (60 timesteps). Since the scenarios only contain vehicle trajectories, ASPILin and Lin use the same data for training and validation, including 61,185 training sequences and 15,164 validation sequences.

C.2 Metrics

Across INTERACTION and CitySim datasets, we forecast future trajectories for $K = 6$ modes and evaluate the model’s performance using Minimum Average Displacement Error (minADE) and Minimum Final Displacement Error (minFDE), denoted as:

$$\text{minADE}_K = \frac{1}{T_f} \min_{k=1}^K \sum_{t=1}^{T_f} \|\hat{y}_t^k - y_t\|_2, \quad (29)$$

$$\text{minFDE}_K = \min_{k=1}^K \|\hat{y}_{T_f}^k - y_{T_f}\|_2. \quad (30)$$

For the highD dataset, we predict a deterministic unimodal trajectory and evaluate the model using Root Mean Square Error (RMSE), expressed as:

$$\text{RMSE} = \sqrt{\frac{1}{NT_f} \sum_{i=1}^N \sum_{t=1}^{T_f} \|\hat{y}_{t,i} - y_{t,i}\|_2^2}, \quad (31)$$

where N represents the total number of samples.

C.3 Implementation Details

Our model is implemented in PyTorch. It uses AdamW as the optimizer, with a cosine annealing scheduler[34], and initial settings for the learning rate, batch size, and training epochs are 1e-3, 64/128/32 for the INTERACTION/highD/CitySim dataset, and 40, respectively. The interaction module’s range threshold \mathcal{D} is set to 30/200/45 meters for the INTERACTION/highD/CitySim dataset. The Transformer used for ablation studies consists of 2 heads, 2 layers, d_z , $d_{z'}$, and the dimensions of the feed-forward module are all set to 256. In our proposed physics-related method, d_z and $d_{z'}$ are configured as 32 and 256, respectively, and the feed-forward module has a dimension of 256. Additionally, we do not set a bias for the linear transformation before the first residual connection to prevent feature confusion caused by zero padding. For the spatiotemporal encoder, the Conv1D kernel size is set to 3, the output channels to 32, and the GRU’s hidden layer dimension to 256. For the map encoder, we use the same settings as HEAT-I-R[39], where \mathcal{M} is a 400×250 grayscale map for each scene, and the details of the scene are shown in Fig. 3. For the three decoders, the hidden layers of $\text{MLP}_\mu(\cdot)$ and $\text{MLP}_\sigma(\cdot)$ are set to (256, 128), and the hidden layer of $\text{MLP}_z(\cdot)$ is set to (1024, 1024). The hidden layer and output dimension of linear transformations $\text{MLP}_{\sigma'}(\cdot)$ are set to (8, 16) and 32, respectively.

ASPILin (3.4M/3.1M/5.7M parameters for the INTERACTION/highD/CitySim dataset) and Lin (2.5M/2.5M/2.8M parameters for the INTERACTION/highD/CitySim dataset) underwent training on a single RTX-4090 and i9-13900K.

D More Experiments

D.1 Inference Speed

Table 7: Inference speed for the INTERACTION/CitySim datasets

Dataset	Model	LP	AS	TP	Total(ms)↓
INTERACTION	Baseline	-	22.29	0.51	22.80
	ASPILin	1.00	8.52	0.24	9.76
CitySim	Baseline	-	6.66	0.79	7.45
	ASPILin	0.99	6.53	0.26	7.78

We evaluate the inference time of the entire prediction process (including Lane Prediction (LP), Agent Selection (AS), and Trajectory Prediction (TP)) of ASPILin on the INTERACTION and CitySim datasets to verify the efficiency of our method and compare it with the baseline (i.e., variant 1 in Tab. 3). Results are shown in Tab. 7. Agent selection consumes most computational resources due

to extensive data processing and conditional filtering, significantly increasing inference time. Even though ASPILin employs more criteria for meticulous agent selection, it remains more efficient than the baseline. This is because the baseline involves extensive data storage operations, taking much more time than needed to make conditional judgments. In the INTERACTION dataset, up to 25 agents can be within 30 meters of the target vehicle, while in the CitySim dataset, there are a maximum of only 5 agents within 45 meters. This explains the discrepancies between ASPILin and the baseline in the two datasets.

Results show that ASPILin possesses high inference efficiency, particularly in scenes with high agent density. While its efficiency slightly underperforms the baseline in scenarios with low agent density, this is completely acceptable. Overall, even if the simultaneous prediction of all vehicle trajectories in a scene is viewed as an aggregation of single-agent predictions, our model performs real-time inference in milliseconds.

E Discussion of Limitations

E.1 Limitations of ASPILin

Essentially, ASPILin is a CVAE model that generates a vehicle’s multi-modal future trajectory in one-shot through reparameterization, which results in some limitations.

Limitation of Single-agent Prediction Although many efforts[39, 23, 11, 9, 22] are dedicated to single-agent prediction, the multi-agent prediction, which involves predicting the trajectories of multiple agents simultaneously, is in fact more in line with real-world requirements. Experiments in App. E.1 have already demonstrated the extremely high inference efficiency of ASPILin, especially in scenarios with high agent density. However, the superiority of multi-agent prediction is evident in its efficiency and ability to simultaneously handle more complex interactions at higher levels. Hence, the majority of single-agent prediction research does not aim to develop an all-encompassing high-performance model, but rather concentrates on advancing or refining one particular aspect, as is the case with ASPILin.

Limitation of CVAE As noted in App. A.2, a limitation of the CVAE model is mode collapse. In this research, we aimed to enhance the diversity of predictions using the loss function $\mathcal{L}_{\text{diversity}}$ represented in Eq. 28; however, the predictions depicted in Fig. 3 similar to many other CVAE models[6, 20, 21, 3] do not demonstrate significant multimodality. It is reasonable because highly multi-modal predictions typically require additional techniques, including maneuver predictions based on classification[25] and transforming the latent space from a single Gaussian distribution to a GMM[22]. However, unthinkingly pursuing high multimodality is not advisable as it enhances the probability of unreliable predictions and could potentially impact the model’s performance[7]. An interesting question is whether highly multi-modal predictions come at the cost of sacrificing prediction accuracy. If so, how do we balance them? The answer to this question is left for future work.

E.2 Limitations of Three Components for Interaction Module

We emphasize that the three components of the interaction module (i.e., agent selection, interaction representation, and interaction encoding) are independent and can be easily integrated into other models. Nevertheless, we still discuss some existing limitations to aid future work.

Limitation of Agent Selection Our method of agent selection is theoretically applicable to any model that involves interaction modeling. However, as it is a lane-related approach, its reliance on high-definition maps renders it inappropriate for models that intentionally do not use maps. A fresh example is ASPILin † in Tab. 1, which does not use maps and selects up to four closest agents around it as interacting agents.

Limitation of Interaction Representation Our research proposes a deterministic interaction representation, but we aim to emphasize the importance of capturing dynamic interactions through this method. Its core idea can be integrated into any other interaction representation. For example, in an interaction representation based on a heterogeneous graph[24, 39], the usual practice is to use a directed edge to determine the interaction between two agents. A mask can be introduced to each

edge to capture dynamic interactions between agents and indicate which agents interact during which periods.

Limitation of Interaction Encoding In Sec. 1, the relationship between agent selection and interaction encoding has been discussed. The limitation of physics-based interaction encoding is that it requires ensuring that the agents who will interact are selected as much as possible. While a coarse agent selection strategy combined with physics-based interaction encoding might enhance model performance because physical coefficients can still represent some agents' interactions, we advise against using this method that sacrifices high interpretability.